

Template synthesis of MnO₂/CNT nanocomposite and its application in rechargeable lithium batteries

ZOU Min-min, AI Deng-jun, LIU Kai-yu

School of Chemistry and Chemical Engineering, Central South University, Changsha 410083, China

Received 17 June 2010; accepted 15 August 2010

Abstract: Nanostructured MnO₂/CNT composite was synthesized by a soft template approach in the presence of Pluronic P123 surfactant. The product was characterized by X-ray diffraction, thermogravimetric and differential thermal analyses, Fourier transformed infrared spectroscopy and high-resolution transmission electron microscopy. The results show that the sample consists of poor crystalline α -MnO₂ nanorods with a diameter of about 10 nm and a length of 30–50 nm, which absorb on the carbon nanotubes. The electrochemical properties of the product as cathode material for Li-MnO₂ cell are evaluated by galvanostatic charge-discharge and electrochemical impedance spectroscopy (EIS). Compared with pure MnO₂ electrode, the MnO₂/CNT composite delivers a much larger initial capacity of 275.3 mA·h/g and better rate and cycling performance.

Key words: MnO₂/CNT; soft template; nanocomposite; rechargeable lithium batteries

1 Introduction

Rechargeable lithium batteries have long been considered an attractive power source for wide applications, ranging from portable electronics to large-scale application such as plug-in hybrid vehicles [1–3]. Various transition metal oxides have been widely studied as electrode materials for rechargeable lithium batteries because of their high theoretical capacity, safety, environmental benignity, and low cost [4–7]. Among transition metal oxides, manganese(IV) oxide is one of the most attractive electrode materials for lithium batteries with environmental friendliness, low cost, and natural abundance [8–9]. However, its potential application in rechargeable lithium batteries is limited by its poor electrical conductivity and large volume expansion during repeated cycling processes [8]. Nanostructured morphologies of these electrodes with controlled crystallinity have been designed to overcome some of these challenges [10–11]. MnO₂/CNTs nanocomposite [12], MnO₂/VACNTs [13] nanocomposite, graphene oxide-MnO₂ nanocrystals [14] and polythiophene/MnO₂ nanocomposite [15] were prepared to improve their capacitive properties. One-dimensional (1D) [16] and three-dimensional (3D) [17]

nanostructured MnO₂ were always synthesized by template method. Template synthesis [18] is a simple and versatile method widely used to obtain nanomaterials and porous structures.

In this study, to combine the merits of template synthesis and the excellent electrical conductivity of CNTs, α -MnO₂/CNTs nanostructure was constructed and prepared by soft template synthesis. Its electrochemical performances in rechargeable lithium batteries were investigated.

2 Experimental

2.1 Synthesis of MnO₂

MnO₂/CNT composite was prepared by a template method in de-ionized water at room temperature. 0.03 g block copolymer P123 was dissolved in 10 mL de-ionized water and mixed with 10 mL 0.4 mol/L MnSO₄ and carbon nanotubes (the theoretical content in the final product is 5%). After being stirred for 12 h, 20 mL solution containing stoichiometric KMnO₄ was added dropwise to the above-mentioned solution and stirred constantly for 24 h. The precipitate was filtered and washed several times, and then dried at 80 °C for 12 h. Finally, the samples were annealed at 350 °C for 6 h to exclude the sample for TGA measurement. For

comparison, the MnO_2 was synthesized without addition of CNTs.

2.2 Characterization

Crystal structure of the manganese oxide was identified by X-ray powder diffraction (D/MAX-IIIC) with a $\text{Cu K}\alpha$ target. Morphology was examined using a scanning electron microscope (JEOL, JSM-6360LV) and a high-resolution transmission electron microscope (JEOL, JEM-3010). Fourier transformed infrared spectroscopy analysis was carried out on a Bruker Equinox55 spectrophotometer (AVATAR360 Nicolet). Thermogravimetric analysis was conducted in N_2 atmosphere at a heating rate of $10\text{ }^\circ\text{C}/\text{min}$ on a thermal analyzer (TGA/SDTA851 $^\circ$, METTLER TOLEDO).

2.3 Electrochemical measurement

The as-synthesized products were employed as cathode active materials for rechargeable lithium-ion cells. The MnO_2/CNT or MnO_2 electrode was composed of 75% (mass fraction) active material, 15% carbon black (containing 5% CNTs) and 10% polytetrafluoroethylene (PTFE). The mixture was pressed into Al foil. The electrodes were dried at $120\text{ }^\circ\text{C}$ in a vacuum furnace for 24 h. The coin cells were assembled using MnO_2 or MnO_2/CNT as working electrode, lithium metal foil as the counter, and 1 mol/L solution of LiPF_6 in 1:1 (V/V) mixture of ethylene carbonate (EC) and dimethyl carbonate (DMC) as electrolyte, and a Celgard 2400 membrane was used as separator.

Electrochemical performance was investigated using the Land 2001A battery measurement system (Wuhan, China). All the laboratory-made Li- MnO_2 cells were charged and discharged at a rate of 30 mA/g between 3.5 and 2.0 V vs Li/Li^+ . EIS tests were conducted by PARSTAT 2273 electrochemical system in the frequency range of 1 MHz–1 mHz, with perturbation amplitude of 5 mV.

3 Results and discussion

3.1 Structure analyses

Figure 1 shows the typical TG-DTA behavior of the synthesized manganese oxide. A mass loss of 16% at temperatures higher than $550\text{ }^\circ\text{C}$ has been detected. The apparent mass loss (about 9%) from room temperature to $200\text{ }^\circ\text{C}$ can be assigned to the loss of absorbed water and crystalline water [19], corresponding to endothermic peaks around $100\text{ }^\circ\text{C}$ and $200\text{ }^\circ\text{C}$, respectively, in the DTA curve. The synthesized MnO_2 decomposes rapidly to form Mn_2O_3 at temperatures beyond $500\text{ }^\circ\text{C}$ [19], and there is a corresponding sharp endothermic peak at

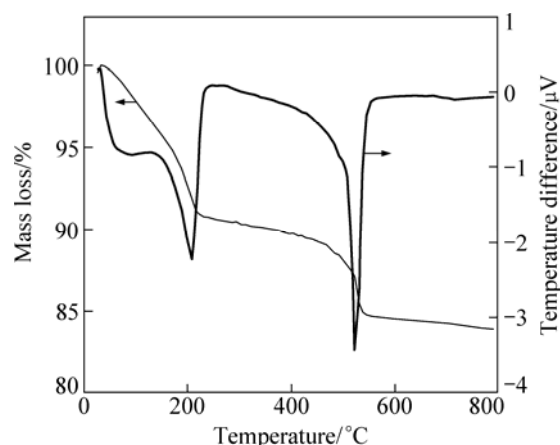


Fig. 1 Typical TG-DTA behavior of synthesized manganese oxide

about $520\text{ }^\circ\text{C}$ in the DTA curve.

Figure 2 shows the XRD patterns of the products after being annealed at $350\text{ }^\circ\text{C}$ for 6 h. The samples were poorly crystallized with broad peaks at 37.1° and 42.6° , indicating the formation of $\alpha\text{-MnO}_2$ (JCPDS No. 44-0141). There are no diffraction peaks of Mn_2O_3 . This confirms that MnO_2 does not decompose to Mn_2O_3 at a temperature of $350\text{ }^\circ\text{C}$ or below, which is in good agreement with the TG-DTA result. The broad diffraction peaks of the sample indicate that its particle size should be small.

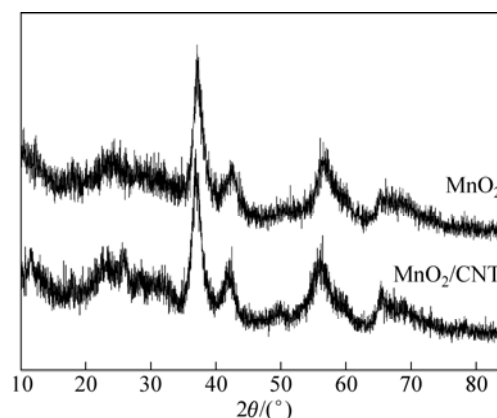


Fig. 2 XRD patterns of as-synthesized products

The FTIR spectrum of the MnO_2/CNT is shown in Fig. 3. The broad peak around 2940 cm^{-1} is attributed to stretching vibration of $\text{H}-\text{O}-\text{H}$ and the weak peaks at about 1080 cm^{-1} , 1540 cm^{-1} and 1602 cm^{-1} are assigned to bending vibration of the $\text{O}-\text{H}$ group, relating to the presence of trace absorbed and crystalline water molecules occluded in the solid during the synthesis of the material [17]. The peak at 513 cm^{-1} can be assigned to the $\text{Mn}-\text{O}$ bending vibration of $\alpha\text{-MnO}_2$ [20–21], which is related to the vibration of MnO_6 octahedron. No peak of P123 was observed, which

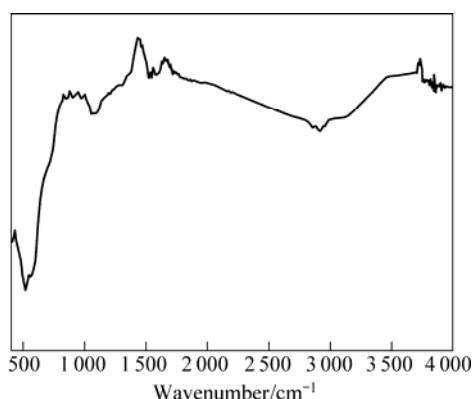


Fig. 3 FTIR spectrum of as-prepared MnO₂/CNT

suggests that the surfactant can be completely removed by washing.

3.2 Morphology characterization

HRTEM images of MnO₂/CNT are presented in Fig. 4. It can be seen that agglomerated MnO₂ particles

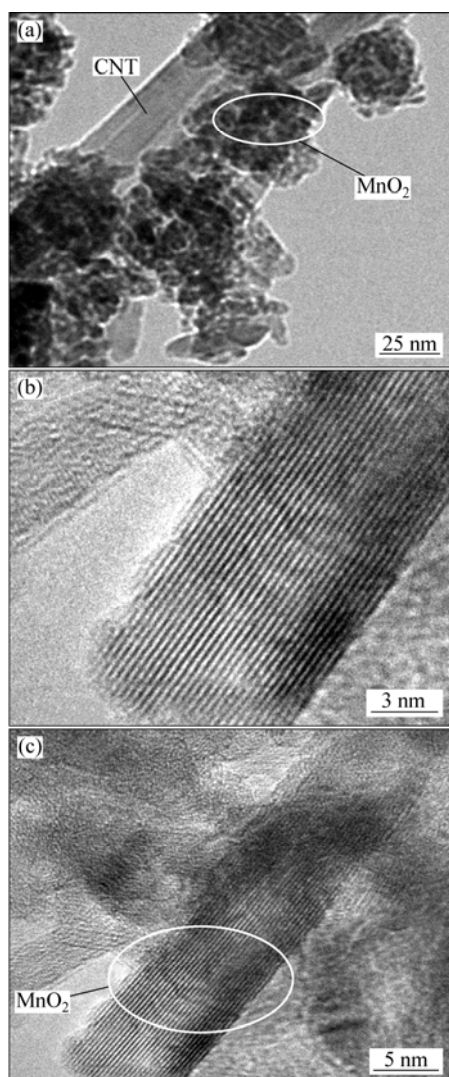


Fig. 4 HRTEM images of MnO₂/CNT: (a) TEM images of MnO₂/CNT; (b), (c) HRTEM images of MnO₂

with an average size of 50–150 nm were attached to the CNTs. The adjacent MnO₂ nanorods are 10 nm in diameter and 30–50 nm in length (Fig. 4(c)), which are mixed together irregularly. The effect of surfactant P123 in this study can be speculated as follows. Mn²⁺ first coordinates with the surfactant to form Mn²⁺-P123 complex. When the Mn²⁺ is oxidized by KMnO₄, the MnO₂ particles grow along the surfactant chains, forming nanorods. These nanorods pile up and form clew shapes, which can be seen in Fig. 4(a).

3.3 Electrochemical characterization

Electrochemical properties of the as-synthesized α -MnO₂ nanostructures were investigated in rechargeable Li-MnO₂ cells. Figure 5 shows the first discharge behaviors and cycling performances of the laboratory-made Li-MnO₂ and Li-MnO₂/CNT cells. Both of the Li-MnO₂ and Li-MnO₂/CNT cells show a flat plateau in the voltage of 2.8 V in the first discharge curves, and the discharge capacities reach 223.4 mA·h/g and 275.3 mA·h/g (The capacity of CNTs is excluded from the electrode in this work), respectively. These values are much higher than those of α -MnO₂ nanofibers

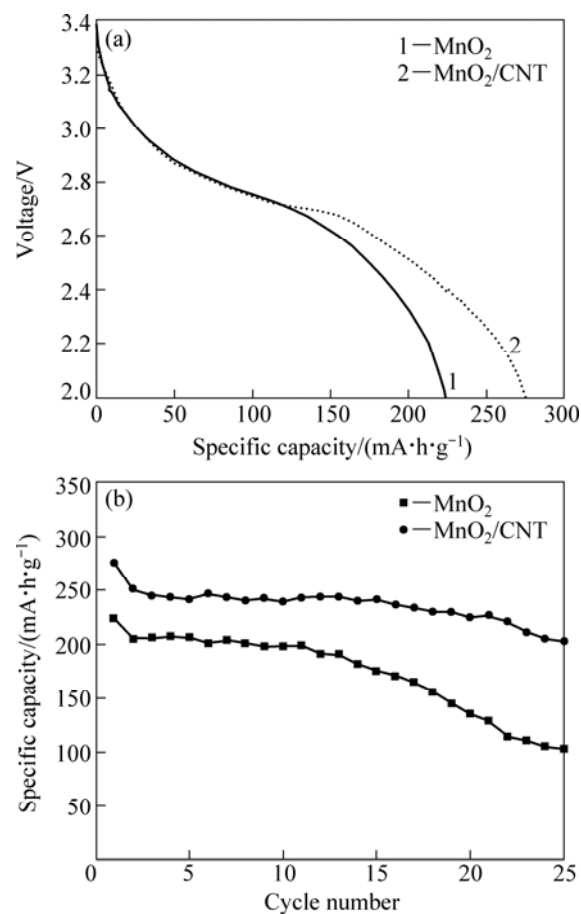


Fig. 5 First discharge curves of MnO₂ and MnO₂/CNT electrodes in Li-MnO₂ cells (a) and discharge capacities of MnO₂ and MnO₂/CNT over the first 25 cycles (b) (Voltage: 3.5–2.0 V, current rate: 30 mA/g)

fabricated by combining template-based method and sol-gel chemistry [22], which delivered a first capacity of 183 mA·h/g and a stabilized capacity of 134 mA·h/g after 10 cycles.

The synthesized MnO₂/CNT also exhibits favorable cyclic stability, and retains a considerable capacity of 203.0 mA·h/g after 25 cycles. The α -MnO₂ delivers a first discharge capacity of 223.4 mA·h/g and retains only 102.9 mA·h/g after 25 cycles, indicating 54% loss of capacity. But we also can see from Fig. 5 that the discharge capacities of the second cycle are much lower than those of the first one. This is likely due to the fact that a fraction of the lithium ions inserted during the initial discharge becomes locked within the crystal structure of MnO₂ for lattice stabilization purpose [22].

The rate performances of the MnO₂ and MnO₂/CNT electrodes were also investigated, their discharge curves and cycling performance are shown in Fig. 6. The discharge capacity of MnO₂ and MnO₂/CNT electrodes at the current rate of 200 mA/g in the range of 3.5–2.0 V are 166.1 mA·h/g and 200 mA·h/g, respectively. After 10 cycles, the capacity retention ratios of MnO₂ and MnO₂/CNT electrodes are 57.5% and 81.5%. The MnO₂/

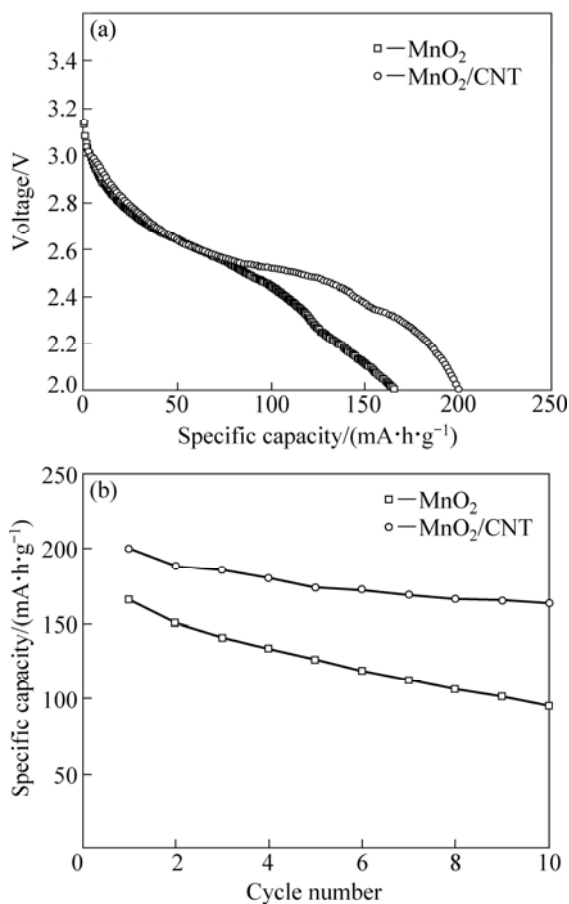


Fig. 6 Discharge curves of MnO₂ and MnO₂/CNT electrodes (a) and their cycling performance (b) at 200 mA/g in range of 3.5–2.0 V

CNT electrode exhibits excellent rate capability and capacity retention.

The enhanced electrochemical performances of the α -MnO₂/CNT can be ascribed to nanorods structures and improved conductivity by inducing highly conductive CNTs. The poor crystalline α -MnO₂ nanorods might possess high surface areas [22], to provide more active sites for the contact between electrode material and electrolyte [23], shortening Li⁺ diffusion distance. The conductive CNTs can facilitate electron transport to the MnO₂ nanorods, and the unique geometric nanostructure and electrical properties of CNTs significantly promote the dispersion of MnO₂ nanorods with strong interaction [24]. So we can conclude that the α -MnO₂/CNT nanostructure is beneficial to faster diffusion kinetics and decreases electrode polarization.

Figure 7 presents typical Nyquist plots of MnO₂ and MnO₂/CNT electrodes obtained before the first discharge. As can be seen from Fig. 7, the MnO₂/CNT electrode has a much smaller charge transfer resistance than the MnO₂ electrode, which indicates that CNTs improve the electrical conductivity of MnO₂ electrode. The smaller charge transfer resistance is also a contributor for the enhanced electrochemical performances mentioned above.

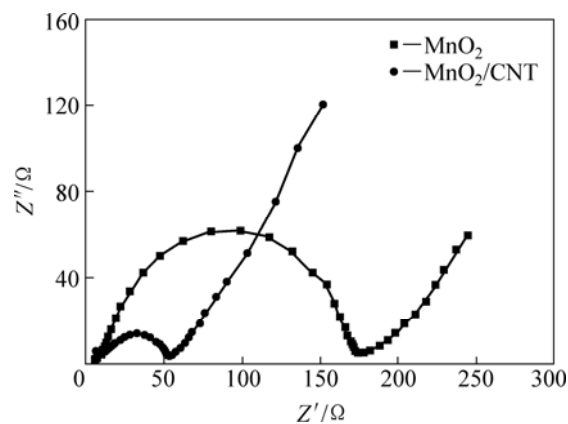


Fig. 7 Electrochemical impedance results of α -MnO₂ and MnO₂/CNT electrodes

4 Conclusions

1) MnO₂/CNT nanocomposite was successfully synthesized by soft template method, and its application for rechargeable lithium batteries was studied.

2) The products have poor crystalline characteristics, and the adjacent nanorods are fused to each other irregularly to form spherical-like agglomerations. The MnO₂ nanorods are absorbed on CNTs in the MnO₂/CNT composite.

3) The MnO₂/CNT electrode delivers a much larger discharge capacity and better cyclic stability and rate capability than pure α -MnO₂.

References

- [1] ARMAND M, TARASCON J M. Issues and challenges facing rechargeable lithium batteries [J]. *Nature*, 2001, 414(6861): 359–367.
- [2] PADHI A K, NANJUNDASWAMY K S, GOODENOUGH J B. Phospho-olivines as positive electrode materials for rechargeable lithium batteries [J]. *Journal of the Electrochemical Society*, 1997, 144(4): 1188–1194.
- [3] CHUNG S Y, BLOKING J T, CHIANG Y M. Electronically conductive phospho-olivines as lithium storage electrodes [J]. *Nature Materials*, 2002, 1(2): 123–128.
- [4] JIAO F, BRUCE P G. Mesoporous crystalline β -MnO₂—A reversible positive electrode for rechargeable lithium batteries [J]. *Advanced Materials*, 2007, 19(5): 657–660.
- [5] POIZOT P, LARUELLE S, GRUGEON S, DUPONT L, TARASCON J M. Nano-sized transition-metal oxides as negative-electrode materials for lithium-ion batteries [J]. *Nature*, 2000, 407(6803): 496–499.
- [6] CHAN C K, PENG H, TWESTEN R D, JARAUSCH K, ZHANG X F, CUI Y. Fast, completely reversible Li insertion in vanadium pentoxide nanoribbons [J]. *Nano Letters*, 2007, 7(2): 490–495.
- [7] SUBRAMANIAN V, BURKE W W, ZHU H, WEI B. Novel microwave synthesis of nanocrystalline SnO₂ and its electrochemical properties [J]. *The Journal of Physical Chemistry C*, 2008, 112(12): 4550–4556.
- [8] DESILVESTRO J, HAAS O. Metal oxide cathode materials for electrochemical energy storage: A review [J]. *Journal of the Electrochemical Society*, 1990, 137(1): 5C–19C.
- [9] KIM D K, MURALIDHARAN P, LEE H W, RUFFO R, YANG Y, CHAN C K, PENG H, HUGGINS R A, CUI Y. Spinel LiMn₂O₄ nanorods as lithium ion battery cathodes [J]. *Nano Letters*, 2008, 8(11): 3948–3952.
- [10] WU M S, CHIANG P C J, LEE J T, LIN J C. Synthesis of manganese oxide electrodes with interconnected nanowire structure as an anode material for rechargeable lithium ion batteries [J]. *The Journal of Physical Chemistry B*, 2005, 109(49): 23279–23284.
- [11] CHENG Fang-yi, TAO Zhan-liang, LIANG Jing, CHEN Jun. Template-directed materials for rechargeable lithium-ion batteries [J]. *Chemistry of Materials*, 2008, 20(3): 667–681.
- [12] YAN Jun, FAN Zhuang-jun, WEI Tong, CHENG Jie, SHAO Bo, WANG Kai, SONG Li-ping, ZHANG Mi-lin. Carbon nanotube/MnO₂ composites synthesized by microwave-assisted method for supercapacitors with high power and energy densities [J]. *Journal of Power Sources*, 2009, 194(2): 1202–1207.
- [13] XU Bin, YE Min-ling, YU Yu-xiang, ZHANG Wei-de. A highly sensitive hydrogen peroxide amperometric sensor based on MnO₂-modified vertically aligned multiwalled carbon nanotubes [J]. *Analytica Chimica Acta*, 2010, 674(1): 20–26.
- [14] CHEN Sheng, ZHU Jun-wu, WU Xiao-dong, HAN Qiao-feng, WANG Xin. Graphene oxide-MnO₂ nanocomposites for supercapacitors [J]. *ACS Nano*, 2010, 4(5): 2822–2830.
- [15] LU Qing, ZHOU Yi-kai. Synthesis of mesoporous polythiophene/MnO₂ nanocomposite and its enhanced pseudocapacitive properties [J]. *Journal of Power Sources*, 2011, 196(8): 4088–4094.
- [16] WANG Xing-hui, NI Shi-bing, ZHOU Guo, SUN Xiao-lei, YANG Feng, WANG Jun-ming, HE De-yan. Facile synthesis of ultra-long α -MnO₂ nanowires and their microwave absorption properties [J]. *Materials Letters*, 2010, 64(13): 1496–1498.
- [17] ZHANG Xiong, YU Peng, CHEN Yao, MA Yan-wei. Low-temperature hydrothermal synthesis of α -MnO₂ three-dimensional nanostructures [J]. *Materials Letters*, 2010, 64(5): 583–585.
- [18] JIANG Rong-rong, HUANG Tao, LIU Jia-li, ZHUANG Ji-hua, YU Ai-shui. A novel nano method to prepare nanostructured manganese dioxide and its electrochemical properties as a supercapacitor electrode [J]. *Electrochimica Acta*, 2009, 54(11): 3047–3052.
- [19] OMOMO Y, SASAKI T, WATANABE M. Preparation of protonic layered manganates and their intercalation behavior [J]. *Solid State Ionics*, 2002, 151(1–4): 243–250.
- [20] YANG Rui-zhi, WANG Zhao-xiang, DAI Lei, CHEN Li-quan. Synthesis and characterization of single-crystalline nanorods of α -MnO₂ and γ -MnOOH [J]. *Materials Chemistry and Physics*, 2005, 93(1): 149–153.
- [21] JULIEN C M, MASSOT M, POINSIGNON C. Lattice vibrations of manganese oxides: Part I. Periodic structures [J]. *Spectrochimica Acta Part A*, 2004, 60(3): 689–700.
- [22] SUGANTHA M, RAMAKRISHNAN P A, HERMANN A M, WARMSINGH C P, GINLEY D S. Nanostructured MnO₂ for Li batteries [J]. *International Journal of Hydrogen Energy*, 2003, 28(6): 597–600.
- [23] CHENG Fang-yi, ZHAO Jian-zhi, SONG Wene, LI Chun-sheng, MA Hua, CHEN Jun, SHEN Pan-wen. Facile controlled synthesis of MnO₂ nanostructures of novel shapes and their application in batteries [J]. *Inorganic Chemistry*, 2006, 45(5): 2038–2044.
- [24] ZHANG Wei-de, XU Bin, JIANG Liao-chuan. Functional hybrid materials based on carbon nanotubes and metal oxides [J]. *Journal of Materials Chemistry*, 2010, 20(31): 6383–6391.

模板法制备纳米 MnO₂/CNT 复合材料 及其在锂电池中的应用

邹敏敏, 艾邓均, 刘开宇

中南大学 化学化工学院, 长沙 410083

摘要: 以 P123 为表面活性剂, 采用软模板法合成 MnO₂/CNT 纳米复合材料。采用 X 射线衍射、热重和差热分析、傅立叶变换红外光谱分析和高分辨率透射电子显微镜对样品进行表征。结果表明, 样品为弱结晶的 α -MnO₂, 直径约 10 nm, 长 30–50 nm, 它们附着在碳纳米管壁上。样品的电化学性能通过组成 Li-MnO₂ 进行电池充放电和电化学阻抗测试(EIS), 与纯二氧化锰相比, MnO₂/CNT 纳米复合材料具有更大的初始容量 275.3 mA·h/g 和更好的倍率和循环性能。

关键词: MnO₂/CNT; 纳米复合材料; 软模板; 锂二次电池

(Edited by LI Xiang-qun)